Real-Time Amplifier Load-Impedance Optimization for Adaptive Radar Transmitters Using a Nonlinear Tunable Varactor Matching Network

SARVIN REZAYAT
Baylor University, Waco, TX USA and National Instruments, Austin, TX USA

CHRISTOPHER KAPPELMANN
Baylor University, Waco, TX USA

ZACHARY HAYS
Baylor University, Waco, TX USA and Raytheon, Waltham, MA USA

LUCILIA LAMERS
Baylor University, Waco, TX USA and Oncor, Dallas, TX USA

MATTHEW FELLOWS
Baylor University, Waco, TX USA and Sandia National Laboratories, Albuquerque, NM USA

CHARLES BAYLIS
Baylor University, Waco, TX USA

ED VIVEIROS
ABIGAIL HEDDEN
JOHN PENN
Army Research Laboratory, Adelphi, MD USA

ROBERT J. MARKS II
Baylor University, Waco, TX USA and Sandia National Laboratories, Albuquerque, NM USA

Manuscript received November 22, 2016; released for publication November 14, 2017. Date of publication July 3, 2018; date of current version February 7, 2019.

DOI. No. 10.1109/TAES.2018.2849198

Refereeing of this contribution was handled by R. Adve.

This work was supported by the Army Research Laboratory under Grant W911NF-16-2-0054. The views and opinions expressed do not necessarily represent the views and opinions of the U.S. Government.

Authors' addresses: S. Rezayat was with Baylor University, Waco, TX 76706 USA. She is now with the National Instruments, Austin, TX 78759 USA, E-mail: (Sarvin_Rezayat@alumni.baylor.edu); C. Kappelmann is with Baylor University, Waco, TX 76706 USA, E-mail: (Christopher_Kappelmann@baylor.edu); Z. Hays was with Baylor University, Waco, TX 76706 USA. He is now with the Raytheon, Waltham, MA 02451 USA, E-mail: (Zach_Hays@alumni.baylor.edu); L. Lamers was with Baylor University, Waco, TX 76706 USA. She is now with the Oncor, Dallas, TX 75202 USA, E-mail: (Luci_Lamers@baylor.edu); M. Fellows was with Baylor University, Waco, TX 76706 USA. He is now with the Sandia National Laboratories, Albuquerque, NM 87185 USA, E-mail: (docfellows@gmail.com); C. Baylis and R. J. Marks II are with the Baylor University, Waco, TX 76706 USA, E-mail: (Charles_Baylis@baylor.edu; Robert_Marks@baylor.edu); E. Viveiros, A. Hedden, and J. Penn are with the Army Research Laboratory, Adelphi, MD 20783, USA, E-mail: (edward.a.viveiros2.civ@mail.mil; abigail.s.hedden.civ@mail.mil; john.e.penn16.civ@mail.mil). *(Corresponding author: Charles Baylis.)*

Future radar transmitters will need to be able to quickly reconfigure their radio-frequency circuitry to change operating frequency and spectral output while maintaining high power-added efficiency (PAE). In this paper, fast tuning of a tunable-varactor matching network is demonstrated to optimize the PAE while meeting requirements on the adjacent-channel power ratio. The tunable varactor network, a first-level prototype of a tunable radar amplifier matching network, incurs nonlinear performance, providing possible challenges to measurement accuracy. To address the issue of nonlinearities while maintaining ability to quickly reconfigure, the tunable-varactor network is characterized at different input power levels to allow useful performance in its nonlinear regime. The power-dependent characterization is used in an algorithm for optimization of an amplifier's PAE, by looking up the matching network characterization performed at the power estimated to be output by the amplifier. Measurement results show that this characterization enhances the consistency of the optimized PAE. Using the tunable varactor network reduces the optimization time to one-fourth of the time required when using the algorithm with a traditional mechanical load-pull tuner.

I. INTRODUCTION

Increasing demands on radar systems, including the need for participating in dynamic spectrum allocation and ability to quickly adapt to changing detection needs, are causing new radar design approaches to be considered for future systems. Cognitive radar has been proposed as a solution [1], [2]. Dynamic spectrum allocation has already become prevalent in many of the radar bands, including the upper part of the radar S-band allocation. Discussions of codesigning the circuit and waveform to meet the increasing demands of a future radar system have been ongoing [3]. Many radar system designers have focused on optimizing the radar waveform, in many situations, with the nonlinear transmitter amplifier "in the loop." Patton and Rigling have created waveform optimization techniques for situations where the autocorrelation and waveform amplitude are constrained [4], where spectrum constraints are present [5], and where the waveform and the matched filter are jointly optimized [6]. Ryan *et al.* have demonstrated hardware-in-the-loop optimization for polyphase coded frequency modulation waveforms in the linear amplification with nonlinear components amplifier topology [7]–[9]. Cognitive radio technology has also been applied to radar applications [10], providing a framework for radar systems to be able to optimize components in "real time," that is, to tune their components during operation for optimum performance, according to their surroundings and needs.

While waveform optimization has been an intense matter of focus, recent attention has been given to design of radar circuitry to support the reconfiguration in next-generation radar systems. Recent work by Guerci and Kingsley has investigated issues of circuit design for cognitive and adaptive radar [11], [12]. One particular roadblock to the implementation of reconfigurable radar transmitters is the power-handling capability of traditional reconfigurable circuit components. While this is beyond the focus of the present paper, parallel developments in high-power tunable components promise that the techniques we present will soon be implementable at power levels needed to accommodate radar transmission [13].

The power amplifier is the largest consumer of energy in the transmitter chain. As a result, its power-added efficiency (PAE) is crucial to the overall power efficiency of the transmitter. As more wireless systems begin to participate in dynamic spectrum allocation, where the operating frequency and bandwidth are allocated to spectrum users in real time, reconfigurable circuitry will be needed to allow the system to operate with excellent efficiency and performance at the frequency assigned for its system's use. A second important characteristic of transmitter devices is to meet standards of adjacent-channel power. This can be assessed by measuring the adjacent-channel power ratio (ACPR) of the device. In this work, we consider the application of tunable matching networks for adaptive power amplifiers, but other networks requiring tunable matching impedances could also use these techniques.

A recent paper by our group shows the design and implementation of a varactor tuning network for an adaptive amplifier [14]. A downfall reported by this work is that the matching network begins to perform nonlinearly at higher values of input power. As a result, the characterization, which determines the load reflection coefficient presented to the amplifier preceding the matching network, is not valid, creating difficulty in optimizing the system clearly, and in assessing the gain and PAE accurately. While a result may still be achieved, nonconvexities in the output power characteristic may cause the algorithm to reach a result that is less than optimal.

Varactor networks have been used for some time in tunable matching networks, and nonlinearities have been a significant problem in the use of tunable matching networks. However, most of the literature focuses on examining the linearity limits of the networks rather than characterizing to allow the networks to operate in their nonlinear regions. Entesari provides a comparison between matching network and filter designs using radio-frequency (RF) microelectrical mechanical systems (MEMS), barium strontium titanate (BST), and GaAs varactors for a WCDMA frontend, and shows that the RF MEMS design has the highest third-order intercept point (IP3), followed by the BST and GaAs varactor designs [15]. Nemati demonstrates the design of tunable varactor networks, and states that nonlinearities in the network are caused by variation of the capacitance values due to the large-signal modulation of the varactor bias voltages [16]. Shen uses two-tone intermodulation measurements in efforts to assess nonlinearity [17], and Hoarau additionally employs 1-dB compression measurements of the matching network [18]. Modeling of the distortion in variable-capacitance diodes is explored by Meyer [19], and Buisman shows that placing varactors in antiseries and antiparallel combinations can mitigate distortion,

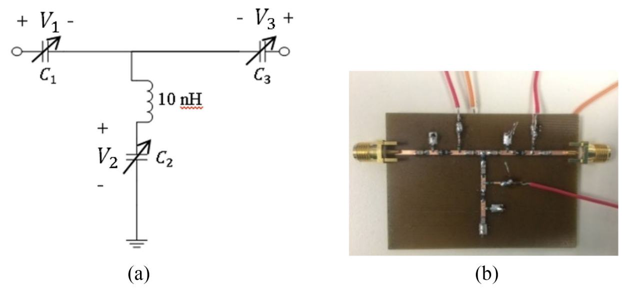

Fig. 1. (a) Design of 1.3 GHz tunable matching network, based on Fu [24]. (b) Implemented tunable-varactor matching network, reprinted from [14] for convenience.

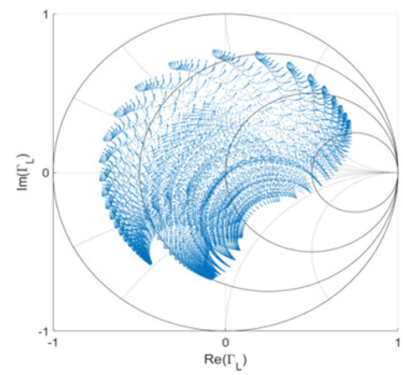

Fig. 2. Characterized load reflection coefficient states for the tunable varactor matching network, reprinted from [14].

validating this with improvements in simulated and measured third-order intermodulation results [20]. Andersson shows how a varactor's behavior can be understood as it is pressed into nonlinearity, and demonstrates a load-pull optimization of the varactor for second-harmonic performance [21]. Park shows that the third-order intermodulation products are a significant function of varactor bias voltage, and states that some varactors can vary by nearly 50% in their capacitance value based on typical bias voltages and large-signal levels [22]. In a 2013 patent, Spears describes the use of a look-up table for reconfigurable impedance matching of an antenna, including the scenarios of precharacterization of matching states over a range of antenna impedances and input power values, among other parameters [23].

Fig. 1 shows the topology and layout of the tunable-varactor matching network, designed for use at 1.3 GHz based on the approach of Fu [24]. Fig. 2 shows the characterized states of the matching network for the load reflection coefficient Γ_L, whose complex plane is the Smith Chart. Fig. 3 shows that, for some values of the varactor diode bias voltages, the gain and other S-parameters significantly vary with input power. This result indicates that the characterization of this varactor tuner is power-dependent. The use of a small-signal characterization of this tuner to predict the Γ_L shown by the tuner, as well as the gain of the tuner in the chain, will result in incorrect results. As such, it is necessary to characterize the tuner at different power levels, and then base the characterization used upon the estimated output power from the transistor. The fast search algorithm

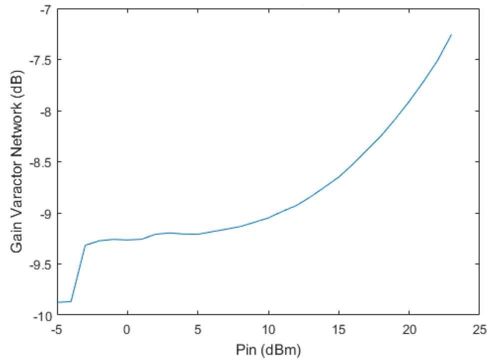

Fig. 3. Measured $|S_{21}|$ versus input power for the varactor matching network at $\Gamma_L = 0.7/\underline{90^\circ}$, reprinted from [14].

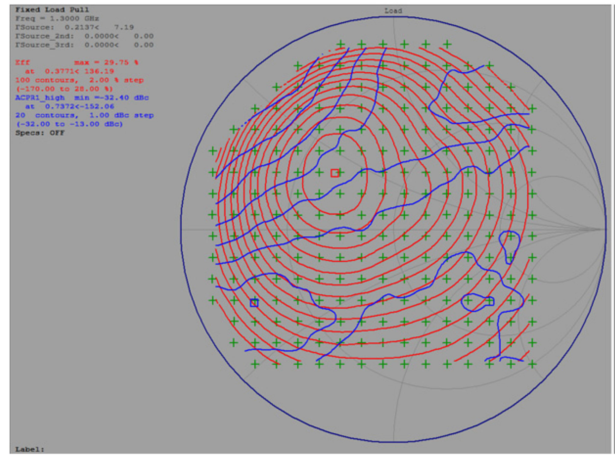

Fig. 4. MWT-173 PAE (red) and ACPR (blue) contours for $V_{\mathrm{GS}} = -1.5$ V, $V_{\mathrm{DS}} = 3$ V, and $P_{\mathrm{in}} = 5$ dBm measured with a Maury Microwave mechanical tuner.

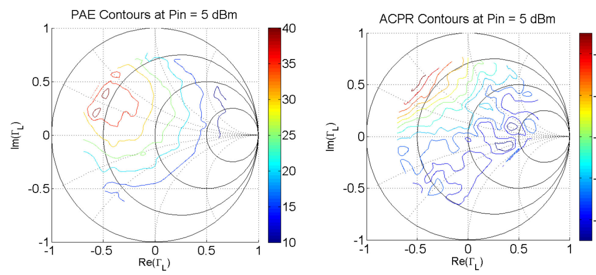

(a) (b)

Fig. 5. MWT-173 PAE (left) and ACPR (right) contours for $V_{\mathrm{GS}} = -1.5$ V, $V_{\mathrm{DS}} = 3$ V, and $P_{\mathrm{in}} = 5$ dBm measured with the tunable-varactor matching network based on a small-signal characterization.

shown in this paper is based on estimated gradients of the PAE and ACPR criteria, as demonstrated by Fellows [25]. Gradient algorithms have been shown to perform reasonably in circuit optimizations of different dimensions [26].

This paper presents a fast search algorithm that can be used for real-time optimization of a tunable-varactor matching network in reconfigurable power amplifiers, including an approach for overcoming power-dependent nonlinearities in the matching network. The results will be applicable in real-time impedance matching with matching networks containing nonlinear devices.

In Section II, load-pull contours taken using the tunable varactor matching network with and without power-dependent characterization at nonlinear power levels are compared to each other and to measurements taken using a traditional Maury Microwave mechanical tuner. The use of the power-dependent characterization in fast load-pull search algorithms designed for real-time constrained optimization is demonstrated in Section III. Some conclusions and suggestions for future work are presented in Section IV.

II. LOAD-PULL RESULTS COMPARISON WITH AND WITHOUT POWER-DEPENDENT CHARACTERIZATION

Comparing load-pull results measured with the tunable-varactor matching network shows improvement by using characterizations performed close to the value of output power expected from the transistor. Measurement comparisons were performed for a Microwave Technologies MWT-173 field-effect transistor (FET) under two different conditions. Fig. 4 shows traditionally measured load-pull results for PAE and ACPR at a bias of $V_{\mathrm{GS}} = -1.5$ V and $V_{\mathrm{DS}} = 3$ V with input power $P_{\mathrm{in}} = 5$ dBm using the Maury Microwave mechanical tuner. These results are expected to be unaffected by the input power level, as the linearity of the mechanical tuners is expected to persist to much higher power levels than those examined in this paper.

For comparison, Fig. 5 shows PAE and ACPR load-pull results measured at the same bias and input-power conditions using the tunable-varactor matching network. The load-pull in Fig. 5 was performed using a standard small-signal characterization of the varactor network. The maximum PAE location predicted by the varactor tuner appears significantly different than the maximum PAE location predicted from measurements with the Maury system. In addition, the maximum PAE value (approximately 35%) obtained from the varactor-tuner load pull is higher than those obtained from the mechanical tuner (approximately 30%).

Because the varactor network is expected to perform nonlinearly at this input power level, a power-dependent characterization of the varactor network was performed. A look-up table was developed based on the power input to the varactor network (output power of the MWT-173 during the load pull). To perform the power-dependent characterization, a gain estimation measurement is performed near each Γ_L point. After estimating gain, the look-up table is used to find the bias voltage combination providing the desired value of Γ_L at the expected device output power (varactor network input power).

Fig. 6 shows the PAE and output power contours obtained by a load-pull measurement using the power-dependent characterization. The PAE optimum location is much closer to the optimum location found with the mechanical-tuner measurement, and the optimum PAE

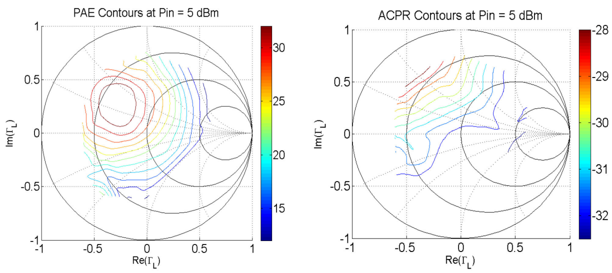

(a) (b)

Fig. 6. MWT-173 PAE (left) and ACPR (right) contours for $V_{\mathrm{GS}} = -1.5$ V, $V_{\mathrm{DS}} = 3$ V, and $P_{\mathrm{in}} = 5$ dBm measured with the tunable-varactor matching network based on a power-dependent characterization.

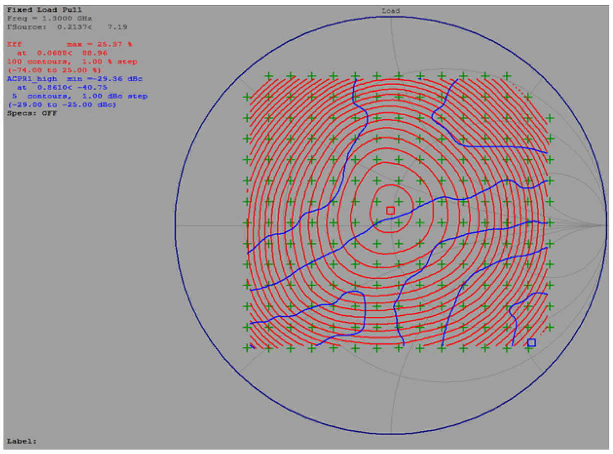

Fig. 7. MWT-173 PAE (red) and ACPR (blue) contours for $V_{\mathrm{GS}} = -1$ V, $V_{\mathrm{DS}} = 2$ V, and $P_{\mathrm{in}} = 4$ dBm measured with a Maury Microwave mechanical tuner.

value is also closer to the optimum PAE found in the mechanical-tuner measurement (approximately 31%).

An investigation as to why the PAE value is overstated when a small-signal characterization is used reveals that as the input power increases, the value of $|S_{21}|$ also has been found to increase for this varactor matching network [14], as shown in Fig. 3. This means that the small-signal measurement for $|S_{21}|$ will be too low, and the de-embedding process of the measured output power from the output of the varactor matching network to the input of the varactor matching network will result in a value that is too large. Thus, the output power and PAE values found at the reference plane between the transistor and matching network will be reported too large when the small-signal characterization is used. In all cases (including the mechanical-tuner load-pull), the ACPR is measured at the spectrum analyzer, so reference plane and characterization are not an issue in the ACPR contours. However, the prediction of the Γ_L values still is less accurate with the small-signal characterization.

Next, a second bias and input-power condition is considered: $V_{\mathrm{GS}} = -1$ V, $V_{\mathrm{DS}} = 2$ V, and $P_{\mathrm{in}} = 4$ dBm. Fig. 7 shows the results of traditional PAE and ACPR load-pull using the mechanical tuner. Fig. 8 shows the PAE and ACPR contours measured using the tunable-varactor matching

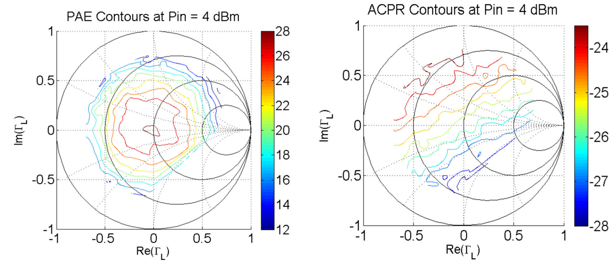

(a) (b)

Fig. 8. PAE (left) and ACPR (right) contours for $V_{\mathrm{GS}} = -1$ V, $V_{\mathrm{DS}} = 2$ V, and $P_{\mathrm{in}} = 4$ dBm measured with the tunable-varactor matching network based on a small-signal characterization

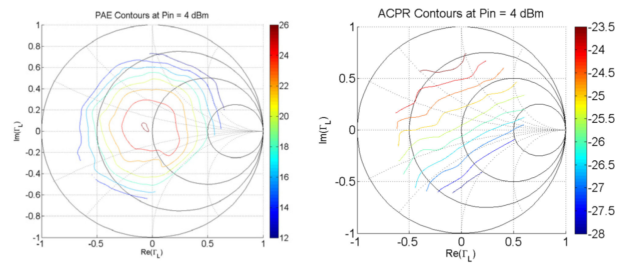

Fig. 9. PAE (left) and ACPR (right) contours for $V_{\mathrm{GS}} = -1$ V, $V_{\mathrm{DS}} = 2$ V, and $P_{\mathrm{in}} = 4$ dBm measured with the tunable-varactor matching network based on a power-dependent characterization.

network with a small-signal characterization, and Fig. 9 shows the contours measured using the tunable-varactor matching network with a power-dependent characterization. A similar phenomenon is observed. The PAE and ACPR contours are not smooth in the load pull taken from small-signal characterization, due to the poor prediction of the Γ_L value presented by the varactor tuner to the transistor under varactor nonlinear conditions. In addition, the predicted optimum PAE value using the small-signal characterization (approximately 28%) is higher than the standard mechanical-tuner load pull (approximately 25%). The power-dependent characterization provides a closer prediction (approximately 26%). For this condition, the small-signal predicted values are not as much in error. This is because the optimum location is near the center of the Smith Chart, where the varactor bias voltages are smaller and less varactor nonlinearity is experienced.

III. FAST LOAD-IMPEDANCE OPTIMIZATION ALGORITHM USING THE VARACTOR MATCHING NETWORK

A fast search for the value of Γ_L providing maximum PAE while maintaining the ACPR below prespecified maximum can be implemented using the varactor tuning network of Fig. 1. This fast search concept, initially demonstrated using the traditional mechanical tuner for fast laboratory load-pull measurements [25], is implemented using the varactor-network for on-the-fly tuning with aid of the power-dependent characterization. This algorithm uses a modified, vector-based gradient search to locate the load reflection coefficient Γ_L providing maximum PAE while

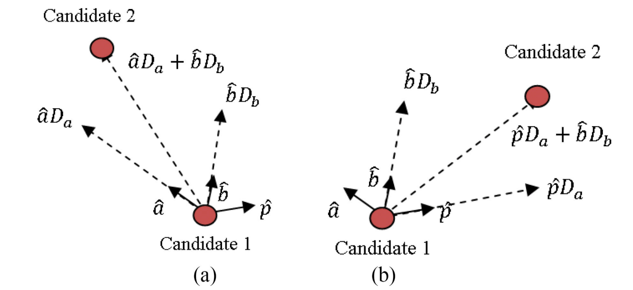

Fig. 10. Search progression, reprinted for convenience [25] for cases when (a) Candidate 1 is outside the ACPR acceptable region and (b) Candidate 1 is inside the ACPR acceptable region.

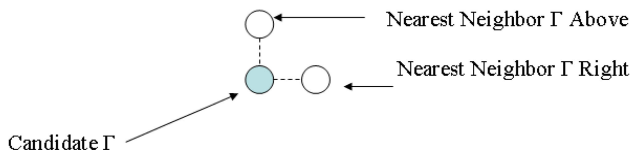

Fig. 11. Estimation of the gradient at a candidate value of Γ_L, reprinted from [25].

remaining below a prespecified ACPR limit. The basic concept of the algorithm [25] is reillustrated in Figs. 10 and 11 for convenience. From the Candidate 1 value of Γ_L, the value of Γ_L for Candidate 2 is selected based on the ACPR steepest-descent direction $\hat{a}$, the PAE steepest ascent direction $\hat{p}$, and the bisector between these vectors $\hat{b}$. To obtain these steepest-ascent and steepest-descent vectors, the gradients are estimated by measuring "neighboring-point" values of Γ_L with respect to the candidate, as shown in Fig. 11 [25].

The power-dependent characterization is used in the algorithm by using an iterative process that selects the appropriate power level and characterization. An initial guess is made to estimate the power input to the varactor network from the output of the device. The characterization that corresponds to the guessed power value is then selected. A measurement of the power is then performed, and using the S-parameters from the characterization associated with the guessed power value, an input power to the varactor network is calculated. If the difference between the initial guess and the measured value are within a certain limit then the process is stopped and that characterization is selected. Otherwise, the guess is set to the measured value and the process is repeated until it converges. Fig. 12 shows a flowchart that summarizes this process. The power-dependent characterization can result in some additional measurements if inaccurate guesses are made.

The algorithm was applied to tune the MWT-173 FET with bias condition $V_{GS} = -1.5$ V, $V_{DS} = 3$ V, and input power $P_{in} = 5$ dBm. For this setting, the goal of the search was to find the Γ_L that maximizes PAE while maintaining ACPR ≤ -30.5 dBc. The algorithm was tested using only a simple small-signal characterization, and then using a power-dependent characterization. Both results are compared to searches using the traditional Maury mechanical tuner.

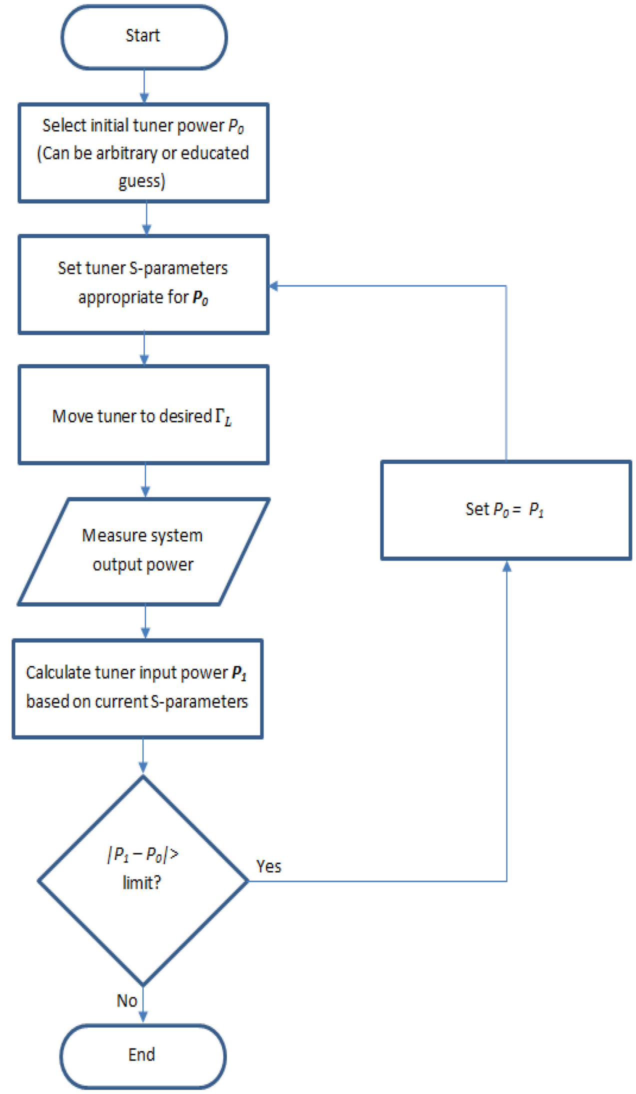

Fig. 12. Flowchart describing the iterative process used to find the appropriate tuner characterization.

Fig. 13 shows the results of a modified gradient search using a small-signal characterization starting at $\Gamma_L = 0.25\underline{/-45^\circ}$. Results from multiple starting points using the small-signal characterization are shown in Table I. The average end PAE value found is 34.4%, with 3.2% PAE standard deviation. The average number of measurements is 13, with an average time per measurement of 4.35 s. It can be seen that the search takes multiple turns; this is consistent with the fluctuating shapes and nonconvexities shown in the Fig. 5 contours. Table I summarizes small-signal characterization search results for multiple Γ_L starting points using this setting.

Fig. 14 shows the search trajectory on the Smith Chart using the power-dependent characterization with the same starting Γ_L ($\Gamma_L = 0.25\underline{/-45^\circ}$) as the small-signal characterization based search shown in Fig. 12. The search path is much more direct than when using the small-signal characterization. Results from multiple starting points for the power-dependent search are shown in Table II. The

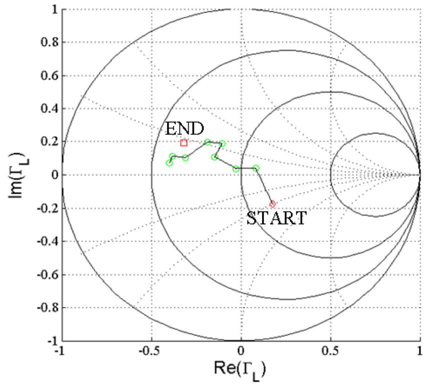

Fig. 13. Search trajectory on the Smith Chart with starting $\Gamma_L = 0.25/\underline{-45^\circ}$ to find the highest PAE with ACPR ≤ -30.5 dBc with a small-signal matching-network characterization. Device conditions are $V_{\mathrm{GS}} = -1.5$ V, $V_{\mathrm{DS}} = 3$ V, and $P_{\mathrm{in}} = 5$ dBm.

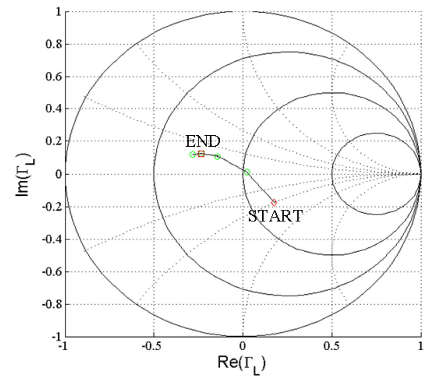

Fig. 14. Search trajectory on the Smith Chart with starting $\Gamma_L = 0.25/\underline{-45^\circ}$ to find the highest PAE with ACPR ≤ -30.5 dBc using a power-dependent matching-network characterization. Device conditions are $V_{\mathrm{GS}} = -1.5$ V, $V_{\mathrm{DS}} = 3$ V, and $P_{\mathrm{in}} = 5$ dBm.

TABLE I
Search Algorithm Results Using Small-Signal Matching Network Characterization for $V_{\mathrm{GS}} = 1.5$ V, $V_{\mathrm{DS}} = 3$ V, and $P_{\mathrm{in}} = 5$ dBm

Start Γ_L	Start PAE (%)	End Γ_L	End ACPR (dBc)	End PAE (%)	# Meas.
0/0°	27.93	0.35/156°	-30.75	36.78	11
0.25/0°	21.66	0.37/115°	-30.66	32.99	13
0.25/45°	26.17	0.33/134°	-30.57	36.43	18
0.25/90°	28.72	0.27/118°	-30.99	33.08	9
0.25/-45°	19.05	0.37/148°	-30.63	37.77	27
0.25/-90°	19.2	0.37/126°	-30.65	36.52	10
0.25/135°	32.54	0.33/122°	-30.93	35.33	8
0.25/180°	29.86	0.33/144°	-30.9	36.05	17
0.25/-135°	24.85	0.41/163°	-30.94	34.63	10
0.5/0°	13.93	0.28/44°	-32.12	25.10	9
0.5/45°	19.51	0.35/135°	-30.71	33.85	14
0.5/90°	28.73	0.44/92°	-30.61	29.23	4
0.5/-135°	18.92	0.37/151°	-31.04	35.07	7
0.5/-90°	13.68	0.33/160°	-31.18	35.00	31
0.5/135°	37.12	0.36/141°	-30.68	36.33	12
0.5/180°	30.76	0.43/157°	-30.79	36.22	8

TABLE II
Search Algorithm Results Using Power-Dependent Matching Network Characterization for $V_{\mathrm{GS}} = -1.5$ V, $V_{\mathrm{DS}} = 3$ V, and $P_{\mathrm{in}} = 5$ dBm

Start Γ_L	Start PAE (%)	End Γ_L	End ACPR (dBc)	End PAE (%)	# Meas
0/0°	26.11	0.37/156°	-30.87	32.44	20
0.25/0°	18.69	0.29/139°	-31.02	32.28	18
0.25/45°	22.42	0.35/125°	-30.54	32.68	19
0.25/90°	28.50	0.26/130°	-30.94	31.96	20
0.25/-45°	18.42	0.27/152°	-31.20	31.93	18
0.25/-90°	18.37	0.41/165°	-31.02	31.30	19
0.25/135°	31.25	0.33/122°	-30.79	31.69	9
0.25/180°	28.16	0.25/128°	-30.85	31.98	9
0.25/-135°	23.79	0.29/136°	-30.85	32.33	19
0.5/0°	12.15	0.28/138°	-30.90	32.25	24
0.5/45°	17.99	0.25/133°	-31.21	32.09	15
0.5/90°	26.06	0.32/133°	-30.76	31.73	21
0.5/-135°	16.46	0.31/139°	-30.76	32.31	20
0.5/-90°	12.80	0.34/131°	-30.70	31.94	20
0.5/135°	32.06	0.26/155°	-31.37	31.91	12
0.5/180°	27.25	0.33/154°	-30.85	32.13	10

average end PAE value found is 32.06%, with .33% PAE standard deviation. The average number of measurements is 13.31, with average time per measurement of 4.4 s. The power-dependent characterization is, in general, expected to require more measurements, due to the need to estimate the output power value at new candidate points for purpose of applying the characterization. When using the small-signal characterization, no estimation of the output power is needed. Another notable difference in comparing the end PAE values is the significantly smaller standard deviation obtained for the power-dependent characterization. This indicates that the convergence of the algorithm is more consistent for the power-dependent characterization than for the small-signal characterization.

Additionally, it can be noted that the PAE values obtained using the small-signal characterization are higher than the PAE values obtained using the power-dependent characterization. This makes sense considering the concept that $|S_{21}|$ increases with increasing input power for high bias voltages (corresponding to Γ_L values on near the upper limit of the Smith Chart). Thus, using a small-signal characterization, the value of $|S_{21}|$ will be underestimated, meaning that the de-embedding of the output power value will be affected in a way that too large of an output value will be reported. As such, the reported PAE is expected to be too large under a small-signal characterization. This is exactly what is observed from comparing the data in Tables I and II.

TABLE III
Search Algorithm Results Using the Mechanical Tuner for $V_{GS} = -1.5$ V, $V_{DS} = 3$ V, and $P_{in} = 5$ dBm

Start Γ_L	Start PAE (%)	End Γ_L	End ACPR (dBc)	End PAE (%)	# Meas
0∠0°	24.79	0.24∠154°	-31.10	29.98	9
0.25∠0°	16.17	0.27∠154°	-30.69	28.43	15
0.25∠45°	23.33	0.23∠156°	-30.74	27.67	12
0.25∠90°	26.78	0.23∠142°	-30.97	30.12	13
0.25∠-45°	16.70	0.30∠149°	-30.68	30.73	15
0.25∠-90°	17.02	0.26∠138°	-30.68	30.51	11
0.25∠135°	30.30	0.28∠151°	-3061	30.44	9
0.25∠180°	27.93	0.28∠149°	-30.54	30.54	9
0.25∠-135°	21.86	0.28∠155°	-30.57	30.20	10
0.5∠0°	11.82	0.22∠141°	-30.67	29.80	16
0.5∠45°	16.80	0.29∠147°	-30.63	30.65	15
0.5∠90°	23.68	0.28∠143°	-30.53	30.69	13
0.5∠-135°	14.97	0.27∠159°	-30.85	29.92	10
0.5∠-90°	8.34	0.24∠148°	-30.56	30.23	14
0.5∠135°	30.27	0.27∠148°	-30.67	30.55	16
0.5∠180°	24.35	0.34∠159°	-30.50	30.22	9

TABLE IV
Comparison of Search Statistics for $V_{GS} = -1.5$ V, $V_{DS} = 3$ V, and $P_{in} = 5$ dBm

	Varactor Network: Power-Dependent Characterization	Varactor Network: Small-Signal Characterization	Mechanical Tuner
Average End PAE (%)	32.06	34.40	30.07
End PAE Standard Deviation (%)	0.33	3.2	0.78
Average End ACPR (dBc)	-30.91	-30.89	-30.69
Average End Γ_L	0.29∠141°	0.35∠134°	0.27∠149°
Average Time Per Measurement (seconds)	3.09	3.12	17.32
Average Number of Measurements	17.06	13	12.25

It is also useful to compare the results of the tunable-varactor load-pull search with results taken by applying the same search algorithm with the Maury Microwave mechanical tuner. Table III shows the results of this load-pull search from multiple starting values of Γ_L.

The results of the searches are compared in Table IV. The average PAE reported using the small-signal characterization is higher than the PAE values reported using the other measurements due to the de-embedding through the varactor network using an incorrect S_{21}, as discussed earlier. In addition, the standard deviation in the end PAE value for the small-signal characterization is high. This is likely due to the fact that the contours are nonconvex and have many curves and ridges, possibly causing the search to be misguided or stop short of the global constrained optimum. The average end Γ_L values show close correspondence between the varactor-network power-dependent characterization results and the results taken with the mechanical tuner. The average end Γ_L from the small-signal characterization is slightly, yet not severely, displaced from these values. The average time per measurement is 3.09 s for the varactor matching network measurements using the power-dependent characterization, compared with an average time per measurement of 17.32 s using the mechanical tuner system. This is a time savings of over 80% in time per measurement. Additional measurements are required, on average, for the varactor network using the power-dependent characterization. This is due to the need to repeat measurements using a different characterization if the guessed output power value is significantly different from the measured result. Because of this issue, approximately four more measurements are required per search for the power-dependent characterization than for the small-signal characterization.

A similar comparison was performed for a second input-power and bias condition: $V_{GS} = -1$ V, $V_{DS} = 2$ V, and $P_{in} = 4$ dBm. For this condition, a constraint of ACPR ≤ -27 dBc was applied. (The contours are shown for the mechanical tuner, varactor tuner small-signal characterization, and varactor tuner power-dependent characterization in Figs. 7–9, respectively.) From a full load-pull measurement using the power-dependent characterization, the best PAE providing ACPR ≤ -27 dBc is 25.34% at $\Gamma_L = 0.28\angle{-45^\circ}$ (see Fig. 9). From a full load-pull measurement using a small-signal characterization, the best PAE providing ACPR ≤ -27 dBc is 24.47% at $\Gamma_L = 0.28\angle{-45^\circ}$ (see Fig. 8). For this bias and input power, the small-signal characterization provides a higher constrained optimum value of PAE. This is due to the interacting shapes of the PAE and ACPR contours as measured in the Smith Chart for the different load-pull results.

Fig. 15 shows the trajectory of the search algorithm in the Smith Chart as performed with the varactor matching network for starting point $\Gamma_L = 0.5\angle 0^\circ$ using the small-signal characterization, and Fig. 16 shows the trajectory for starting point $\Gamma_L = 0.5\angle 45^\circ$ using the power-dependent characterization with the varactor matching network. Table V shows the results of fast searching from multiple starting Γ_L values using the varactor matching network with a small-signal characterization. Table VI shows the results of fast searching from the same starting Γ_L values using the varactor matching network with a power-dependent characterization. Table VII shows the results of fast searching using a traditional mechanical load-pull tuner. Table VIII compares the results from the different searches.

The common conclusion that can be drawn by examining the search summary comparisons in Table VIII is that the varactor tuning network converges to consistent PAE values with a higher degree of repeatability for the large-signal characterization than for a small-signal

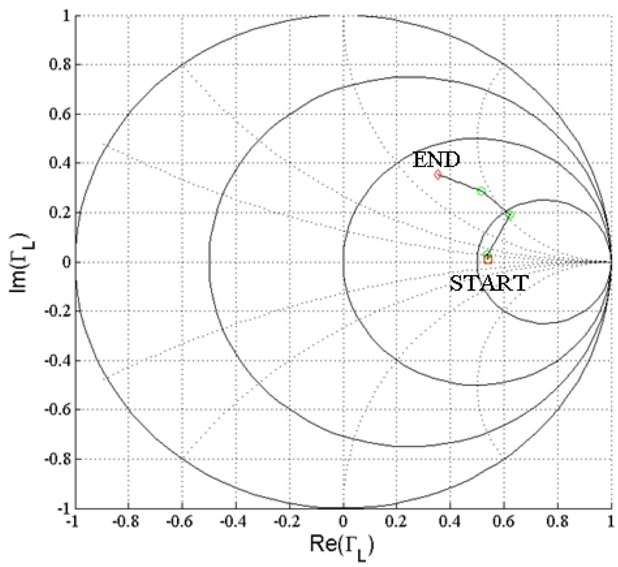

Fig. 15. Search trajectory on the Smith Chart with starting $\Gamma_L = 0.5/\underline{0°}$ to find the highest PAE with ACPR ≤ -27 dBc with a small-signal matching-network characterization. Device conditions are $V_{GS} = -1$ V, $V_{DS} = 2$ V, and $P_{in} = 4$ dBm.

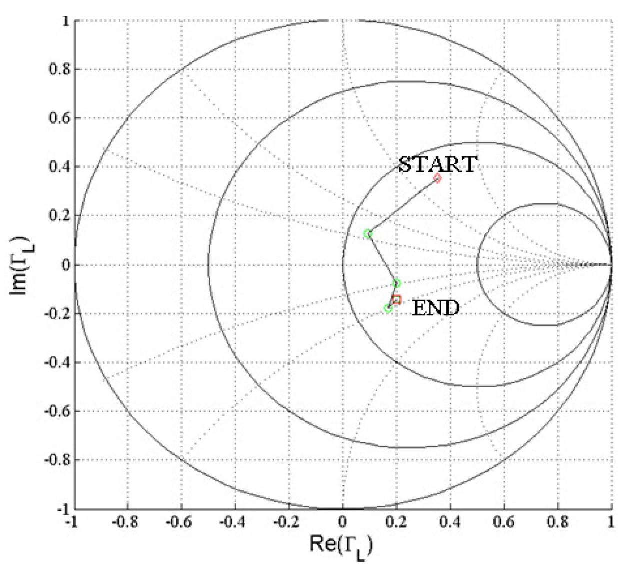

Fig. 16. Search trajectory on the Smith Chart with starting $\Gamma_L = 0.5/\underline{45°}$ to find the highest PAE with ACPR ≤ -27 dBc using a power-dependent matching-network characterization. Device conditions are $V_{GS} = -1$ V, $V_{DS} = 2$ V, and $P_{in} = 4$ dBm.

characterization. Similar to the first set of operating conditions used, the end PAE standard deviation is much smaller for the large-signal characterization than for the small-signal characterization. Due to the inaccuracy of the small-signal characterization to predict the value of Γ_L presented to the load, as well as the other S-parameters, the values obtained for the PAE vary significantly. While the gradient algorithm used shows remarkable robustness to the nonconvexities introduced by an inaccurate characterization (seen in Fig. 5 and 8), the results end up varying slightly. Additionally, it can be noted that the time per measurement in the varactor-network search is approximately one-fifth of the time per measurement for a traditional mechanical tuner and software package.

TABLE V
Search Algorithm Results Using Small-Signal Matching Network Characterization for $V_{GS} = -1$ V, $V_{DS} = 2$ V, and $P_{in} = 4$ dBm

Start Γ_L	Start PAE (%)	End Γ_L	End ACPR (dBc)	End PAE (%)	# Meas.
0/0°	28.31	0.26/-56°	-27.13	24.06	7
0.25/0°	26.36	0.32/-32°	-27.40	25.29	13
0.25/45°	26.87	0.32/-34°	-27.50	25.29	16
0.25/90°	25.99	0.28/-50°	-27.18	25.55	11
0.25/-45°	24.9	0.32/-34°	-27.41	25.28	15
0.25/-90°	23.96	0.34/-30°	-27.62	24.93	12
0.25/135°	26.21	0.31/-59°	-27.22	24.48	10
0.25/180°	26.04	0.21/-59°	-27.15	24.84	7
0.25/-135°	26.14	0.29/-92°	-27.18	23.20	7
0.5/0°	19.66	0.29/-45°	-27.17	25.65	14
0.5/45°	21.12	0.54/1°	-27.21	18.09	13
0.5/90°	21.56	0.39/-10°	-27.23	23.54	17
0.5/-135°	20.38	0.36/-99°	-27.24	23.38	10
0.5/-90°	19.43	0.40/-98°	-27.27	22.51	9
0.5/135°	22.77	0.23/-60°	-27.34	24.18	16
0.5/180°	21.49	0.46/-109°	-27.22	21.20	16

TABLE VI
Search Algorithm Results Using Power-Dependent Matching Network Characterization for $V_{GS} = -1$ V, $V_{DS} = 2$ V, and $P_{in} = 4$ dBm

Start Γ_L	Start PAE (%)	End Γ_L	End ACPR (dBc)	End PAE (%)	# Meas
0/0°	28.26	0.23/-36°	-27.08	25.09	11
0.25/0°	25.22	0.31/-28°	-27.20	24.44	8
0.25/45°	25.67	0.28/-42°	-27.26	25.50	12
0.25/90°	26.42	0.30/-50°	-27.42	24.94	15
0.25/-45°	25.10	0.25/-45°	-27.05	25.10	5
0.25/-90°	25.56	0.22/-40°	-27.04	25.72	13
0.25/135°	26.62	0.24/-66°	-27.36	24.48	12
0.25/180°	26.29	0.24/-72°	-27.22	24.80	10
0.25/-135°	26.02	0.31/-46°	-27.55	24.96	11
0.5/0°	18.82	0.24/-38°	-27.07	25.02	20
0.5/45°	21.14	0.25/-36°	-27.02	25.12	17
0.5/90°	21.33	0.34/-16°	-27.02	24.38	21
0.5/-135°	20.03	0.34/-99°	-27.24	24.28	15
0.5/-90°	19.78	0.34/-92°	-27.06	24.40	9
0.5/135°	19.14	0.26/-95°	-27.03	24.21	22
0.5/180°	19.96	0.33/-93°	-27.12	24.37	18

While it appears that the power-dependent characterization helps to hone the results for higher accuracy, it also appears that that a useful result for real-time reconfigurable radar is reached with the varactor matching network even

TABLE VII
Search Algorithm Results Using the Mechanical Tuner for $V_{GS} = -1$ V, $V_{DS} = 2$ V, and $P_{in} = 4$ dBm

Start Γ_L	Start PAE (%)	End Γ_L	End ACPR (dBc)	End PAE (%)	# Meas
0/0°	25.15	0.26/-24°	-27.07	22.44	10
0.25/0°	23.07	0.27/-30°	-27.19	22.14	12
0.25/45°	23.70	0.24/-35°	-27.12	22.60	22
0.25/90°	24.37	0.30/-10°	-27.05	22.04	16
0.25/-45°	22.06	0.25/-45°	-27.08	22.06	5
0.25/-90°	21.62	0.24/-44°	-27.21	22.18	12
0.25/135°	23.36	0.29/-19°	-27.07	22.07	19
0.25/180°	22.65	0.33/-105°	-27.02	20.29	22
0.25/-135°	22.54	0.24/-60°	-27.13	21.89	10
0.5/0°	17.27	0.23/-29°	-27.11	22.74	14
0.5/45°	17.60	0.39/-14°	-27.24	19.75	13
0.5/90°	19.63	0.23 /-36°	-27.06	22.26	31
0.5/-135°	15.73	0.36/-109°	-27.02	18.18	9
0.5/-90°	14.87	0.27/-44°	-27.15	21.63	8
0.5/135°	17.10	0.23/-34°	-27.11	22.53	31
0.5/180°	14.84	0.24/-34°	-27.15	21	16

TABLE VIII
Comparison of Search Statistics for $V_{GS} = -1$ V, $V_{DS} = 2$ V, and $P_{in} = 4$ dBm

	Varactor Network: Large-Signal Characterization	Varactor Network: Small-Signal Characterization	Mechanical Tuner
Average End PAE (%)	24.80	23.84	21.61
End PAE Standard Deviation (%)	0.45	1.96	1.23
Average End ACPR (dBc)	-27.12	-27.28	-27.11
Average End Γ_L	0.25/-55°	0.31/-63°	0.24/-42°
Average Time Per Measurement (seconds)	3.49	3.47	19.23
Average Number of Measurements	13.68	12.06	15.62

when a small-signal characterization is used. A significant time savings is accomplished by using the varactor tuner, regardless of the characterization. Requirement of 3–4 s per measurement is primarily due to equipment overhead, which will be significantly reduced in a real-time optimization from a cognitive radio platform in an adaptive radar.

IV. CONCLUSION

A constrained optimization for the PAE under ACPR constraints has been demonstrated using a tunable-varactor matching network. The varactor matching network can tune to provide repeatable results for the optimization from multiple starting reflection coefficient values, requiring approximately one-fifth of the time per measurement required by a traditional bench-top load-pull tuner. This matching network serves as a first-level prototype of a reconfigurable matching network to be used in an adaptive radar transmitter. Further, the results show that the use of a power-dependent characterization can account for nonlinearities in the tuner itself, providing more consistent and accurate search results. In many cases, more measurements are required for the power-dependent characterization due to needed repeated measurements when an error in power estimation is incurred. The fast reconfiguration time and accuracy of this tuning algorithm will allow the radar to adapt in a congested environment to coexist with communication and other radar systems. Parallel developments in high-power tunable passive components are expected to allow this algorithm to be useful in real-time radar transmitter optimization.

ACKNOWLEDGMENT

The authors would like to thank J. Clark of the Army Research Laboratory for his helpful comments and assistance.

REFERENCES

[1] S. Haykin
Cognitive radar: A way of the future
IEEE Signal Process. Mag., vol. 23, no. 1, pp. 30–40, Jan. 2006.

[2] J. Guerci
Cognitive Radar: The Knowledge-Aided Fully Adaptive Approach. Norwood, MA, USA: Artech House, 2010.

[3] H. Griffiths, S. Blunt, and L. Savy
Challenge problems in spectrum engineering and waveform diversity
In *Proc. IEEE Radar Conf.*, Ottawa, ON, Canada, Apr./May 2013, pp. 1–3.

[4] L. K. Patton and B. D. Rigling
Autocorrelation and modulus constraints in radar waveform optimization
In *Proc. Int. Waveform Diversity Des. Conf.*, Kissimmee, FL, USA, Feb. 2009, pp. 150–154.

[5] L. K. Patton and B. D. Rigling
Phase retrieval for radar waveform optimization
IEEE Trans. Aerosp. Electron. Syst., vol. 48, no. 4, pp. 3287–3302, Oct. 2012.

[6] L. K. Patton and B. D. Rigling
Autocorrelation constraints in radar waveform optimization for detection
IEEE Trans. Aerosp. Electron. Syst., vol. 48, no. 2, pp. 951–968, Apr. 2012.

[7] L. Ryan, J. Jakabosky, S. D. Blunt, C. Allen, and L. Cohen
Optimizing polyphase-coded FM waveforms within a LINC transmit architecture
In *Proc. IEEE Radar Conf.*, Cincinnati, OH, USA, May 2014, pp. 835–839.

[8] S. D. Blunt, J. Jakabosky, M. Cook, J. Stiles, S. Seguin, and E. L. Mokole
Polyphase-coded FM (PCFM) radar waveforms, Part II: Optimization
IEEE Trans. Aerosp. Electron. Syst., vol. 50, no. 3, Jul. 2014, pp. 2230–2241.

[9] J. Jakabosky, L., Ryan, and S. Blunt
Transmitter-in-the-loop optimization of distorted OFDM radar emissions
In *Proc. IEEE Radar Conf.*, Ottawa, ON, Canada, Apr./May 2013, pp. 1–5.

[10] H. Deng and B. Himed
Interference mitigation processing for spectrum sharing between radar and wireless communication systems
IEEE Trans. Aerosp. Electron. Syst., vol. 49, no. 3, pp. 1911–1919, Jul. 2013.

[11] N. Kingsley and J. R. Guerci
Adaptive amplifier module technique to support cognitive RF architectures
In *Proc. IEEE Radar Conf.*, Cincinnati, OH, USA, May 2014, pp. 1329–1332.

[12] N. Kingsley and J. R. Guerci
Radar RF Circuit Design. Norwood, MA, USA: Artech House, 2016.

[13] A. Semnani and D. Peroulis
Nano-plasma tunable evanescent-mode cavity resonators
In *Proc. IEEE MTT-S Int. Microw. Symp.*. Tampa, FL, USA, Jun. 2014, pp. 1–3.

[14] Z. Hays *et al.*
Real-time amplifier optimization algorithm for adaptive radio using a tunable-varactor matching network
In *Proc. IEEE Radio Wireless Symp.*, Phoenix, AZ, USA, Jan. 2017, pp. 215–217.

[15] K. Entesari and G. M. Rebeiz
RF MEMS, BST, and GaAs varactor system-level response in complex modulation systems
Int. J. RF Microw. Comput.-Aided Eng., vol. 18, no. 1, pp. 86–98, Jan. 2008.

[16] H. M. Nemati, C. Fager, U. Gustavsson, R. Jos, and H. Zirath
Design of varactor-based tunable matching networks for dynamic load modulation of high power amplifiers
IEEE Trans. Microw. Theory Techn., vol. 57, no. 5, pp. 1110–1118, May 2009.

[17] Q. Shen and N. S. Barker
Distributed MEMS tunable matching network using minimal-contact RF-MEMS varactors
IEEE Trans. Microw. Theory Techn., vol. 54, no. 6, pp. 2646–2658, Jun. 2006.

[18] C. Hoarau, N. Corrao, J.-D. Arnold, P. Ferrari, and P. Xavier
Complete design and measurement methodology for a tunable RF impedance matching network
IEEE Trans. Microw. Theory Techn., vol. 56, no. 11, pp. 2620–2627, Oct. 2008.

[19] R. G. Meyer and M.-L. Stephens
Distortion in variable-capacitance diodes
IEEE J. Solid-State Circuits, vol. 10, no. 2, pp. 47–54, Feb. 1975.

[20] K. Buisman *et al.*
Distortion free varactor diode technologies for RF adaptivity
In *Proc. IEEE MTT-S Int. Microw. Symp.*, Long Beach, CA, USA, Jun. 2005, pp. 157–160.

[21] C. M. Andersson, M. Thorsell, and N. Rorsman
Nonlinear characterization of varactors for tunable networks by active source-pull and load-pull
IEEE Trans. Microw. Theory Techn., vol. 59, no. 7, pp. 1753–1760, Jul. 2011.

[22] S.-J. Park and G. M. Rebeiz
Low-loss two-pole tunable filters with three different predefined bandwidth characteristics
IEEE Trans. Microw. Theory Techn., vol. 56, no. 5, pp. 1137–1148, May 2008.

[23] J. H. Spears, W. E. Smith, C. Sui, and Y. Zhu
Methods for Tuning an Adaptive Impedance Matching Network With a Look-Up Table. U.S. Patent 8,421,548, 2013.

[24] J.-S. Fu and A. Mortazawi
Improving power amplifier efficiency and linearity using a dynamically controlled tunable matching network
IEEE Trans. Microw. Theory Techn., vol. 56, no. 12, pp. 3239–3244, Dec. 2008.

[25] M. Fellows, C. Baylis, J. Martin, L. Cohen, and R. J. Marks II
Direct algorithm for the pareto load-pull optimization of power-added efficiency and adjacent-channel power ratio
IET Radar, Sonar Navig., vol. 8, no. 9, pp. 1280–1287, Dec. 2014.